Int. J. Electrochem. Sci., 14 **(2019)** 4595 – 4610, doi: 10.20964/2019.05.37

International Journal of
ELECTROCHEMICAL
SCIENCE
www.electrochemsci.org

PEDOT: PSS-exfoliated Graphene to Improve the Corrosion Resistance of Waterborne Epoxy Coating

Yue Su[1,2], *Shihui Qiu*[1,2], *Yu Liu*[1], *Dongping Yang*[1], *Haichao Zhao*[1,*], *Liping Wang* [1,*]

[1] Key Laboratory of Marine Materials and Related Technologies, Zhejiang Key Laboratory of Marine Materials and Protective Technologies, Ningbo Institute of Materials Technology and Engineering, Chinese Academy of Sciences, Ningbo 315201, P. R. China
[2] University of Chinese Academy of Sciences, Beijing 100049, China
[*]E-mail: zhaohaichao@nimte.ac.cn, wangliping@nimte.ac.cn

Received: 2 January 2019 / *Accepted:* 11 February 2019 / *Published:* 10 April 2019

In this paper, we prepared PEDOT:PSS-G composites on the basis of π-π interactions between PEDOT:PSS and graphene. It was revealed that PEDOT:PSS has been inserted into the graphene sheets and graphene sheets were peeled off into 4-5 layers by SPM analysis. Electrochemical impedance spectroscopy and micro-electrochemical spectrum showed the agglomerated graphene not only couldn't act as barriers, but also accelerated the corrosion reaction; while the exfoliated graphene fully exerted its barrier effect and increased the diffusion path for corroded medium. Meanwhile, the addition of PEDOT:PSS could promote the formation of passivation layers on the steel surface, and inhibited the corrosion reaction from further occurring. The two effects complemented each other to improve the corrosion resistance of the coating.

Keywords: Graphene; PEDOT:PSS; Corrosion inhibition; Cooperative effect

1. INTRODUCTION

Graphene is a sp^2-hybridized two-dimensional layered material [1], which possesses extremely high specific strength, large specific surface areas, gas barrier and oxidation resistance [2], excellent anti-wear performances, etc [3, 4]. And it has aroused the attention of researchers due to the excellent physicochemical properties and been widely used in electrical, optical, biochemical and other fields [5, 6]. The high impermeability of graphene can prevent oxygen, water, and corrosive ions (such as chloride ions) from contacting with metal substrates, and act as a physical shield [7]. Studies have shown that single or multi-layered graphene coatings can provide good protection for metals against thermal, wet, and electrochemical corrosion [8-10]. Defect-free single-layer graphene can act as an excellent corrosion protection barrier due to its impervious property, yet high-quality sheets could only be synthesized on

the particular substrate with the complicated conditions [11, 12]. Moreover, Schriver et al. and Zhou et al. [13, 14] found that CVD-grown graphene coating only provided effective short-term oxidation protection, but it took an accelerated effect on the wet corrosion even over the originally unprotected Cu surface. Graphene was deposited on the copper surface by chemical vapor deposition, which had a large number of defects. When it was in a corrosive environment for a long time, oxygen, water and corrosive ions passed through the defects, contacted with the copper surface and caused the corrosion of the copper foil. Compared to uncoated samples, graphene's high electrical conductivity transferred electrons to the relatively inert cuprous oxide surface, which could exacerbate corrosion and cause localized severe corrosion.

Another way is to use graphene as the functional filler in an organic resin. However, graphene can be easy to agglomerate and has poor dispersibility in resin due to its strong interlayer interaction force. Up to now, it is possible to improve the dispersibility of graphene by covalent method and non-covalent method. The covalent bond method is to graft molecules onto the surface of graphene oxide by chemical reaction. Luo et al. [15] prepared by in situ synthesis and salt formation reaction, which dispersed stably in water and epoxy resin. Li et al. [16] first synthesized a boronated boron nitride ($BN(OH)_X$) functionalized p-phenylenediamine-modified reduced graphene oxide (rGO) filler ($BN(OH)_X$-PrGO). The $BN(OH)_X$-PrGO/PU composite film has excellent oxygen barrier properties, ideal dielectric properties and excellent anticorrosive performances. Bahram Ramezanzadeh et al. [17] synthesized polyaniline-CeO_2 grafted graphene oxide sheets through layer by layer self-assembly method. The results show that graphene oxide deposited with polyaniline and CeO_2 has improved barrier and active corrosion inhibition performances. Zheng et al. [18] prepared graphene oxide-poly(urea-formaldehyde) (GUF) composite by immobilizing a pre-polymer of urea-formaldehyde resin on a graphene oxide (GO) sheet through in-situ polycondensation. The UF resin on the surface of the GO sheet converted the hydrophilic GO sheet into a hydrophobic GUF composite, which improved the compatibility of composite with the coating, and prevented the aggregation of GUF during ball milling. Graphite oxide was covalently modified with 3-aminopropyl trimethoxysilane to improve the dispersion of graphene oxide in epoxy resin. Feng et al. [19] covalently modified graphene oxide with 3-aminopropyl trimethoxysilane (APTMS-GO) to improve the dispersion of GO in epoxy resin. A wide variety of chemical modification methods have been studied, these methods not only improved the hydrophobicity of graphene but also endue it with new properties. However, the methods of chemical modifications were complicated to synthesize and were not environmentally friendly; more importantly, they would destroy the graphene sheet structure and affect its barrier properties. The π-π interaction improved the dispersibility of graphene, and the operation was simple and environmentally friendly. This method has attracted more and more researchers' attention. Yuan et al. [20] successfully prepared a series of few layer graphene modified waterborne epoxy resin dispersions by using lipophilic surfactants hydrophilic epoxy oligomer as dispersants. Yang et al. [21] combined 3,4,9,10-perylenebenzoic acid (PTCA) and graphene (G) by π-π interaction and hydrophobic force. The synthesis process of small molecule surfactants was complicated and the effect was single. The conductive polymers had dense π-electron clouds and were ideal materials for graphene dispersion. Chen et al. [22] used poly(2-butylaniline) (P2BA) as a dispersant to achieve the stable dispersion of graphene in THF by non-covalent π-π interaction between P2BA and graphene nanosheets. Qiu et al. [23] used π-π interaction

between polypyrrole and graphene, and the stacked graphene sheets were peeled off to a thickness of three to five layers without increasing defects. Non-covalent interactions could not only improve good dispersion of graphene but also form oxide passivation layers on the surface of metals.

Poly(3,4-ethylenedioxythiophene) (PEDOT) is intrinsic conducting polymers (ICP) [24], and usually combined with poly(styrenesulfonate) (PSS) to increase its solubility. PEDOT:PSS is widely used in the research of organic solar cell materials [24], OLED materials [25], electrochromic materials [26] and transparent electrode materials [27]. The substituted thiophene rings leads to larger steric hindrance, resulting in the rigid polymer chain and fewer conjugate defects; furthermore the conductivity of PEDOT is not very high [28-30], which can reduce the possibility that the conductive polymer and graphene are interconnected to form a conductive path.

In this article, we use poly(3,4-ethylenedioxythiophene)-poly(styrenesulfonate) (PEDOT:PSS) as a non-covalent dispersant to obtain graphene composite coating. Meanwhile PEDOT: PSS accelerates the formation of a passivation oxide layer at the interface between the metal material and the organic coating to protect the metal from corrosion.

2. EXPERIMENT SECTION

2.1 Materials

Poly(3,4-ethylenedioxythiophene)-poly(styrenesulfonate) (PEDOT:PSS) was purchased from Sigma-Aldrich Co. Ltd. Graphene was purchased from Changzhou Sixth Element Co. Ltd. Epoxy (E44) and waterborne curing agent were bought from Yunda Chemical Co. Ltd. China. Anhydrous ethanol was bought from Sinopharm Chemical Reagent Co. Ltd. All the chemicals were used without further purification, and deionized water was employed in the total experiment.

2.2 Preparation of PEDOT:PSS-graphene hybrid

A certain amount of PEDOT:PSS was dissolved in 5 mL of the mixture of deionized water and ethanol (V:V=1:1), and ultrasonically dispersed for 1 hour to obtain a deep blue aqueous solution. Subsequently, a certain amount of graphene was added to the above PEDOT:PSS solution, and the mixture was ultrasonicated for 1 hour. The mass ratio of graphene and PEDOT:PSS is 2:1.

2.3 Fabrication of composite coatings

Before coating, Q235 electrodes with an exposed area of 1 cm^2 were sanded with 600 and 1200 mesh sandpaper and rinsed with deionized water. After ultrasonically removing surface grease and other substances with ethanol and acetone, electrodes were dried under nitrogen and then saved in a vacuum oven. The PEDOT:PSS-graphene hybrid was firstly evaporated to remove most of the solvent and then centrifuged at 3000 rpm for 5 minutes. The slurry was mixed fully with the pre-calculated epoxy resin via mechanical agitation, and then removed residual solvent with a rotary evaporator. With the curing agent (epoxy: curing agent=4:1) added, the compound was mixed entirely under the high speed mixer at

5000 rpm for 2 min and degassed in a vacuum oven for 30 seconds. The slurry was applied to the electrode surfaces with a wire rod, and the samples were cured at room temperature for three days. The samples named as pure-coating, G-coating and PG-coating were prepared in the similar way as control sample. The coating thickness was measured by using a thickness gauge (FY2050) device to be 53 ± 2 μm.

2.4 Materials characterization

The physical properties of PEDOT:PSS, G and PEDOT:PSS-G hybrid were characterized by UV-vis spectroscopy (Lambda 950) and Raman spectroscopy (Renishaw inVia Reflex). The elemental composition and chemical structure of hybrid materials were analyzed by X-ray photoelectron spectroscopy (AXIS-ULTRA XPS). Crystal characteristics were analyzed by X-ray diffractometer (XRD, Bruker D8 Advance) using 40 KV, 30 mA Cu Kα (λ=0.154 nm) radiation. Microscopic morphology was presented via scanning probe microscopy (SPM, Dimension 3100) and transmission electron microscopy (TEM, TF-20) and field emission scanning electron microscope (SEM, Hitachi S4800). The dispersion of graphene in the coating was characterized by Raman surface scanning. The morphology of the coating fracture surface and the steel surface after corrosion were observed by field emission scanning electron microscopy (SEM, Quanta 250).

2.5 Electrochemical measurement

The coated carbon steel was immersed in 3.5 wt% NaCl solution and the samples were measured by a ModuLab electrochemical workstation (Solartron). The workstation is equipped with a typical three-electrode device including a platinum counter electrode (board area is 2.5 cm^2), a reference electrode (saturated calomel electrode (SCE)) and a working electrode. Impedance measurements were recorded using an alternating current signal with the amplitude of 10 mV over a frequency range of 100 kHz to 0.01 Hz. The local corrosion state of the coating was evaluated by scanning vibrating electrode technique. A probe with the diameter of 50 μm was used to vibrate in the vertical direction of the surface at the frequency of 80 Hz and amplitude of 30 μm (peak to peak). The scanning area was 3 mm × 3 mm, and the scanning steps in the X and Y directions were both 0.1 mm.

2.6 Salt spray test

In line with the ASTM B117 standard, the corrosion resistance of the composite coating was investigated by salt spray test.

3. RESULTS AND DISCUSSION

3.1 Proof of PEDOT:PSS-G Hybrids

Graphene is abbreviated as G, and PEDOT:PSS-G hybrid is abbreviated as PG. Figure 1 showed the preparation process of PEDOT:PSS-G hybrid composites. The π-π interaction between graphene and

PEDOT:PSS resulted in the separation of graphene sheets. 10 mL of graphene solution (C_G=5 mg/mL) and 10 mL of PG solution (C_{PG}=5 mg/mL, m_G:$m_{PEDOT:PSS}$=2:1) were shown in Figure 1. As can be seen from the picture, Graphene appeared to sink to the bottom, but the picture of PG solution showed a homogeneous solution, which illustrated the dispersibility of graphene was significantly improved.

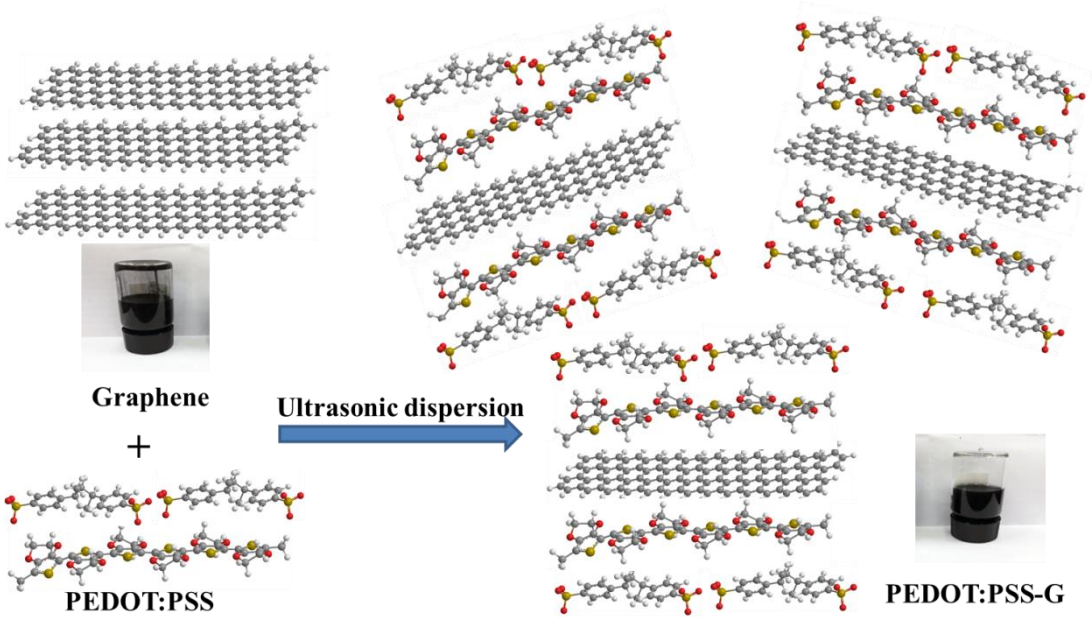

Figure 1. Schematic representation of the preparation of PEDOT:PSS-G hybrids

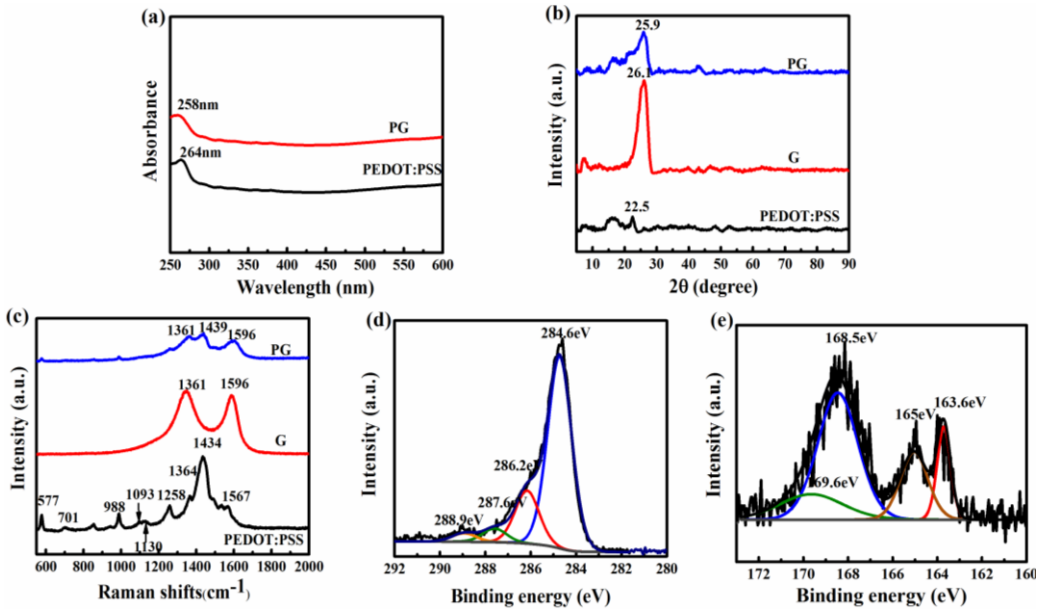

Figure 2. (a).UV-vis spectra of PEDOT:PSS and PEDOT:PSS-G, (b).XRD patterns and (c) Raman spectra of PEDOT:PSS, graphene and PEDOT:PSS-G, XPS fine spectrum of (d) C 1s and (e) S 2p.

The graphene was directly dispersed in ethanol, agglomeration and precipitation were apt to occur due to the strong interlayer van der Waals interactions. PEDOT:PSS could be used as a dispersant

to achieve good dispersion of graphene in ethanol. The π-π interactions between PEDOT:PSS and graphene were analyzed by UV-vis , X-ray diffraction, Raman spectroscopy and X-ray photoelectron spectroscopy.

Figure 2a showed the UV absorption peaks of PEDOT:PSS and PEDOT:PSS-G hybrids in solution. The absorption peak of PEDOT appeared nearly 264 nm, which corresponded to π-π transition of thiophene [31]. Compared with PEDOT:PSS, the π-π transition of hybrids was blue shifted to 260 nm, which testified the π-π interaction between PEDOT and graphene [23].

In Figure 2b, graphene possessed a crystallization peak at 26.5°, revealing the calculated in-plane spacing was 0.340 nm. After inserting PEDOT:PSS, the peak shifts to 25.9° and the in-plane spacing became 0.343 nm [23]. Graphene presented the D and G peaks at 1361 cm^{-1} and 1596 cm^{-1} (Figure 2c), which were ascribed to carbon atom lattice defects and carbon atom sp^2 hybrid in-plane stretching vibration, respectively [32-34]. In terms of PEDOT:PSS, the main peaks included symmetrical C–S–C deformation (701 cm^{-1}), oxyethylene ring deformation (577 and 988 cm^{-1}), C–O–C deformation (1093 cm^{-1}), C–C interring tension (1258 cm^{-1}), single C–C tension (1364 cm^{-1}), C=C symmetric tension (1434 cm^{-1}), C=C asymmetric tension (1490 cm^{-1}) and C=C antisymmetric tension (1567 cm^{-1}) [35-40]. Compared with PEDOT, the C=C symmetric stretching vibration of hybrid materials moved from 1434 cm^{-1} to 1439 cm^{-1}, indicating that there was a strong π-π interaction between the graphene and PEDOT:PSS molecules [39-40]. As shown in Figure 2d, the peaks of the fine carbon spectrum presented C–C/C=C (284.6 eV), C(C=O)R (285.7 eV) and O–C=O (288.7 eV) [41]. The S 2p spectrum of PEDOT:PSS-G (Figure 2e) showed emission signals at 163.6 eV, 165 eV, 168.5 eV and 169.6 eV, which were consistent with the S2p peak of PEDOT:PSS reported in the literature; the peak at 166 to 171 eV could be deconvolved into two spin splitting doublets: the peaks at 168.4 and 169.6 eV corresponded to the PSS-Na^+ [42-43]. The S2p emission peaks at 163.7 and 165.04 eV belonged to PEDOT [42-43].

3.2 Morphology analysis

SEM, TEM and SPM were applied to observe the morphology of the composites. As shown in Figure 3a and 3c, the sheets of pristine graphene were thick and easy to fold and agglomerate. After the intercalation, the sheet became thinner than before in Figure 3b and 3d. The thicknesses of PEDOT:PSS-G measured by SPM were 1.17 nm and 2.267 nm (Figure 3e-3f).

The uniformity of graphene in organic matrix can be characterized by Raman mapping. Figure 4 shows a conspicuous decrease in the distribution density, it was found that the dispersibility of PEDOT:PSS-G in the resin was significantly improved [44]. In Figure 4c, pure epoxy resin possessed smooth cross section, but the cross-section of graphene-based resin was uneven (Figure 4d) due to the agglomeration of graphene in resin. Meanwhile they all had manifest holes owning to the evaporation of solvent and crack propagation [23]. Figure 4e exhibited the cross section of the PEDOT:PSS-G coating. Compared with Figure 4d, the cross-section was distinctly smoother and sparse cracks

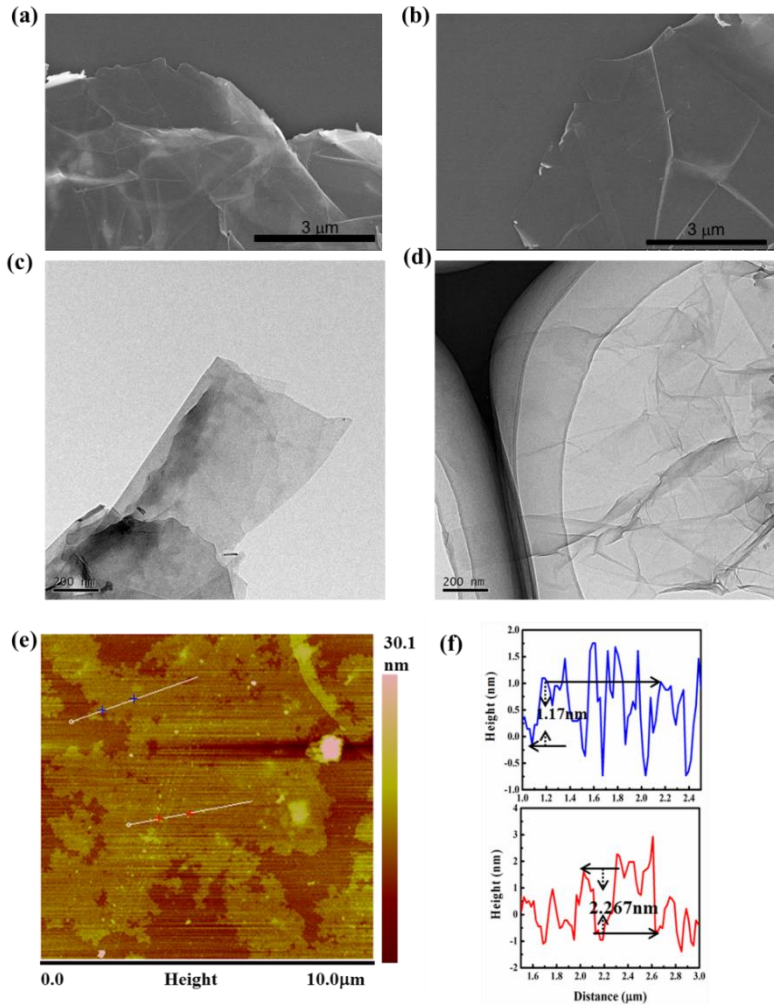

Figure 3. SEM images of (a) G and (b) PEDOT:PSS-G; TEM images of (c) G and (d) PEDOT:PSS-G; (e,f) SPM image of PEDOT:PSS-G.

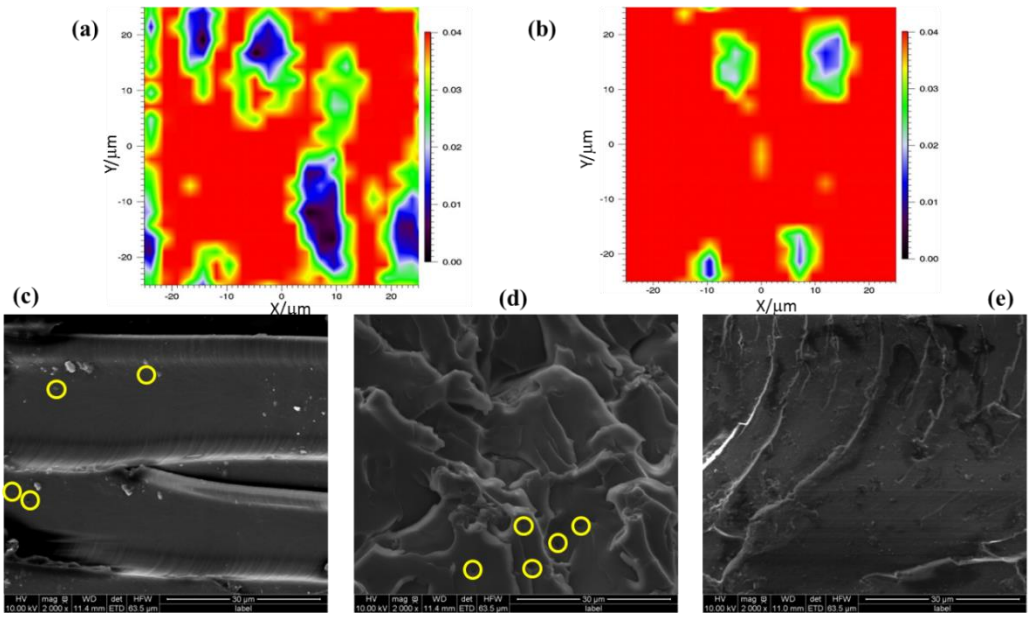

Figure 4. (a, b) Raman mapping desity of G-coating and PG-coating; the sectional SEM images of (c) pure-coating, (d) G-coating and (e) PG-coating.

3.3 Electrochemical analysis

The electrode was immersed in a 3.5 wt% NaCl solution for 60 days. The electrochemical impedance spectroscopy of the coatings was shown in Figure 5. In general, the impedance modulus of the lowest frequency (Z_f=0.01 Hz) in the Bode plot can be used as a semi-quantitative indicator of the barrier properties of the coating [45]. The low frequency impedance of pure epoxy resin was 1.73×10^9 Ω cm^2, and it was reduced to 7.58×10^5 Ω cm^2 after soaking for 60 days. For pure epoxy coating (Figure 5a$_1$), the phase angle value at low-middle frequency region (10^{-2}–100 Hz) is closed to 0° in an extended frequency region with the immersion, indicating the metal basement gradually lost the protection and suffered from corrosion.

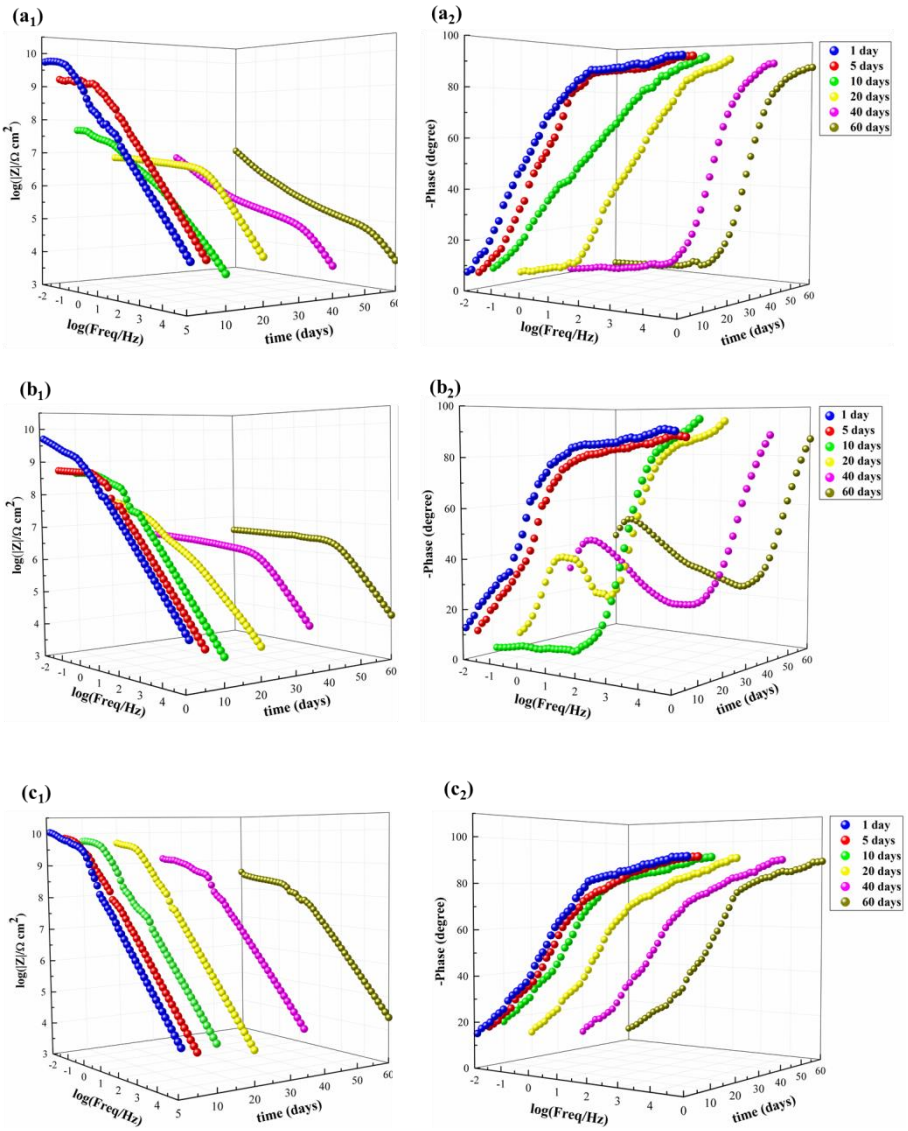

Figure 5. The electrochemical impedance spectroscopy of (a_1, a_2) pure-coating, (b_1, b_2) G-coating and (c_1, c_2) PG-coating.

For the coating with G and PG, the initial low frequency impedances were 4.45×10^9 Ω cm^2 and 1.05×10^{10} Ω cm^2 respectively, which were higher than that of pure epoxy resin. Over 60 days of

immersion, the low frequency impedances of coating with G and PG were 3.62×10^6 Ω cm^2 and 1.35×10^9 Ω cm^2. The Bode-phase plots at 10 days for G-coating sample show the similar tendency with the pure epoxy coating, but the responsive peak for corrosion reaction appears after the immersion of 10 days and tends to move to the low frequency. It conveyed a signal that corrosive medium reaches to the interface between coating and substrate. When the electrodes were immersed for 33 days, the low frequency impedance of the G-coating (3.4×10^6 Ω cm^2) was lower than that of the pure coating (5.4×10^6 Ω cm^2), indicating that the graphene coating has been damaged (consistent with the electrochemical simulation circuit), corrosive mediums penetrated into the interior of the coating and the agglomerated graphene may form a conductive path that accelerated corrosion process. As the soaking time increased, the surface oxidation products acted as protective layers and the impedances of the coatings increased slightly. The impedances of the PEDOT:PSS-G coatings were maintained at 10^9 Ω cm^2 until the end of the immersion and the protective properties of the coating remained well.

To further investigate electrochemical behavior, we simulated the electrochemical equivalent circuit by using ZsimDemo 3.30 software. Figure 6a and 6b were electrochemical analog circuit diagrams. The electrical equivalent circuit was composed of R_c, R_s and Q_c, which represented coating resistance, solution resistance and coating capacitance, respectively. And coating resistances are used to evaluate the barrier properties of the coatings [23]. When the coating is damaged, the electrochemical behavior of the steel interface consists of charge transfer resistance (R_{ct}) and electric double layer capacitance (Q_{dl}) [45, 46]. Charge transfer resistors describe the degree of charge transfer on metal surfaces and are inversely proportional to the rate of corrosion. R_{ct} value decreases with the immersion time increased, which indicates that the corrosion reaction under the coating is underway. Corrosive electrolytes and water gradually reach the metal surfaces through cracks or pores of the coating to diffuse on the steel surface and cause severe metal corrosion. Since the metal/solution interface is not a true capacitor, there are interface effect and capacitance deviation, so a better fit can be obtained by using a CPE (constant phase element) instead of the double layer capacitor Q_{dl} [47-50]; CPE satisfies the following formula:

$$Z_{CPE} = [f_0 (j\omega)^n]^{-1}$$

where f_0 is the scale factor of CPE, w is the angular frequency, and j is the imaginary number, n represents the index of CPE; if n = 1, the constant phase constant is equal to the coating capacitance. Coating capacitance meets the formula: $C_{dl}=Y_0(\omega_{max})^{n-1}$, ω_{max} is the frequency corresponding to the imaginary part of the maximum impedance (Z").

In Figure 6c, the coating resistance for pure epoxy coating gradually decreased with the time increased, indicated the declined protective properties of coating. In terms of G-coating, the coating resistance began to gradually decrease and then remained unchanged or slightly increased during the immersion, implying that the surface oxidation products played a certain protective role. After comparison, it was found that the PG coating exhibited the highest resistance, because the addition of PEDOT played a good dispersion effect and improved the barrier properties of the resin.

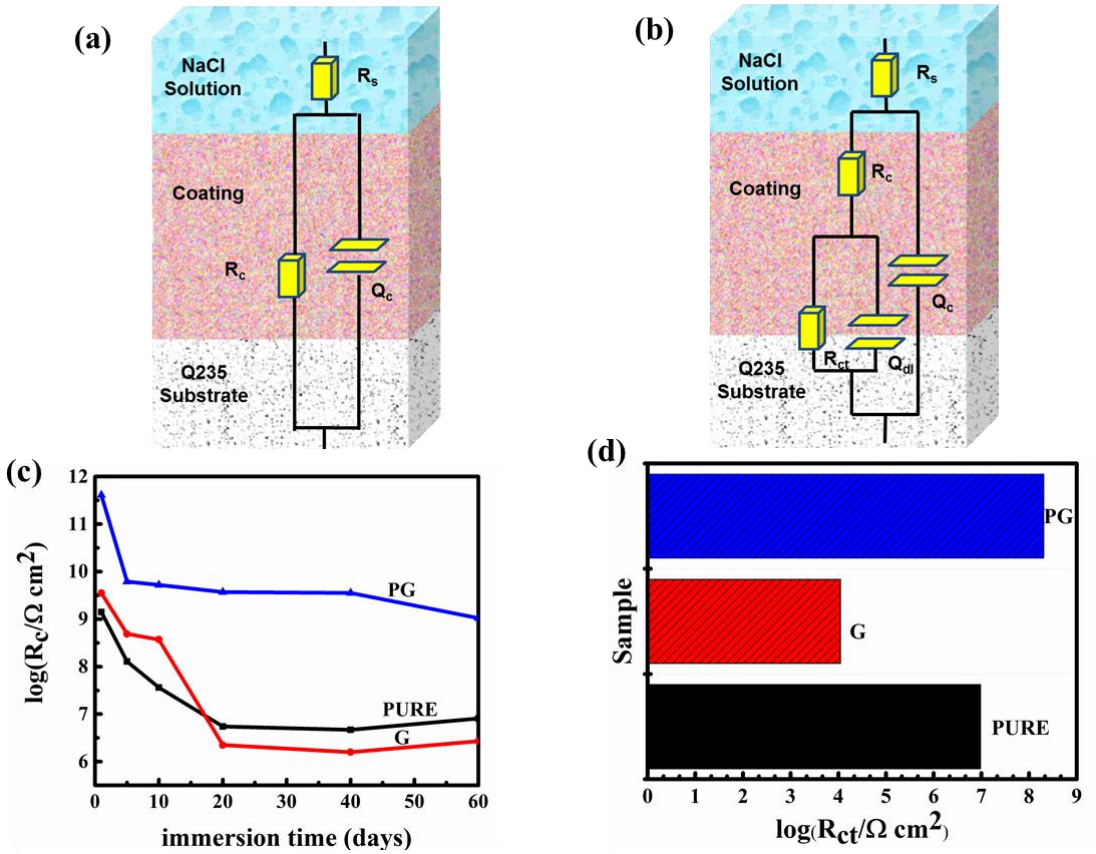

Figure 6. (a-b) Electrical equivalent circuit models. (c) Evolution of Rc with immersion in 3.5 wt% NaCl solution, (d) Charge transfer resistances when immersed for 20 days.

Figure 6d displayed that charge transfer resistance for G-coating was the smallest, implying the fastest corrosion rate. It was detected that the addition of graphene could improve the barrier property of coating, but on the other hand, the agglomerated graphene may form a conductive path to accelerate the metal corrosion. After soaking for a period of time, the pure resin coating was destroyed, and corrosion products were formed a protective layer on the substrate but its structure was not dense and couldn't completely block the corrosion reaction.

3.4 Study on self-healing properties of coatings

The local electrochemical behavior of the coating was studied by scanning vibrating electrode technology. The relationship between voltage drop and local current density satisfies the ohmic formula: $J=-\Delta\Phi Kd^{-1}$, K represents the conductivity of 3.5 wt% NaCl solution, $\Delta\Phi$ is the voltage drop, and d is the amplitude of vibration electrode [23]. For pure epoxy coatings, the highest anode current density increased from 0.165 to 0.272 μA cm^{-2}; for the G-coatings, the anode corrosion current density increased from 0.224 to 0.585 μA cm^{-2}, and undispersed graphene accelerated the corrosion of the coating. For PG-coating, the highest anode corrosion current density increased from 0.165 to 0.224 μA cm^{-2} with the least increase, and compared the 6-hour with 24-hour chart, we discovered that the cathode current density of the coating increased when the electrode was immersed for 24 hours. PEDOT:PSS could not

only promote the formation of a passivation layer on the steel surface but also inhibited the anode reaction [51].

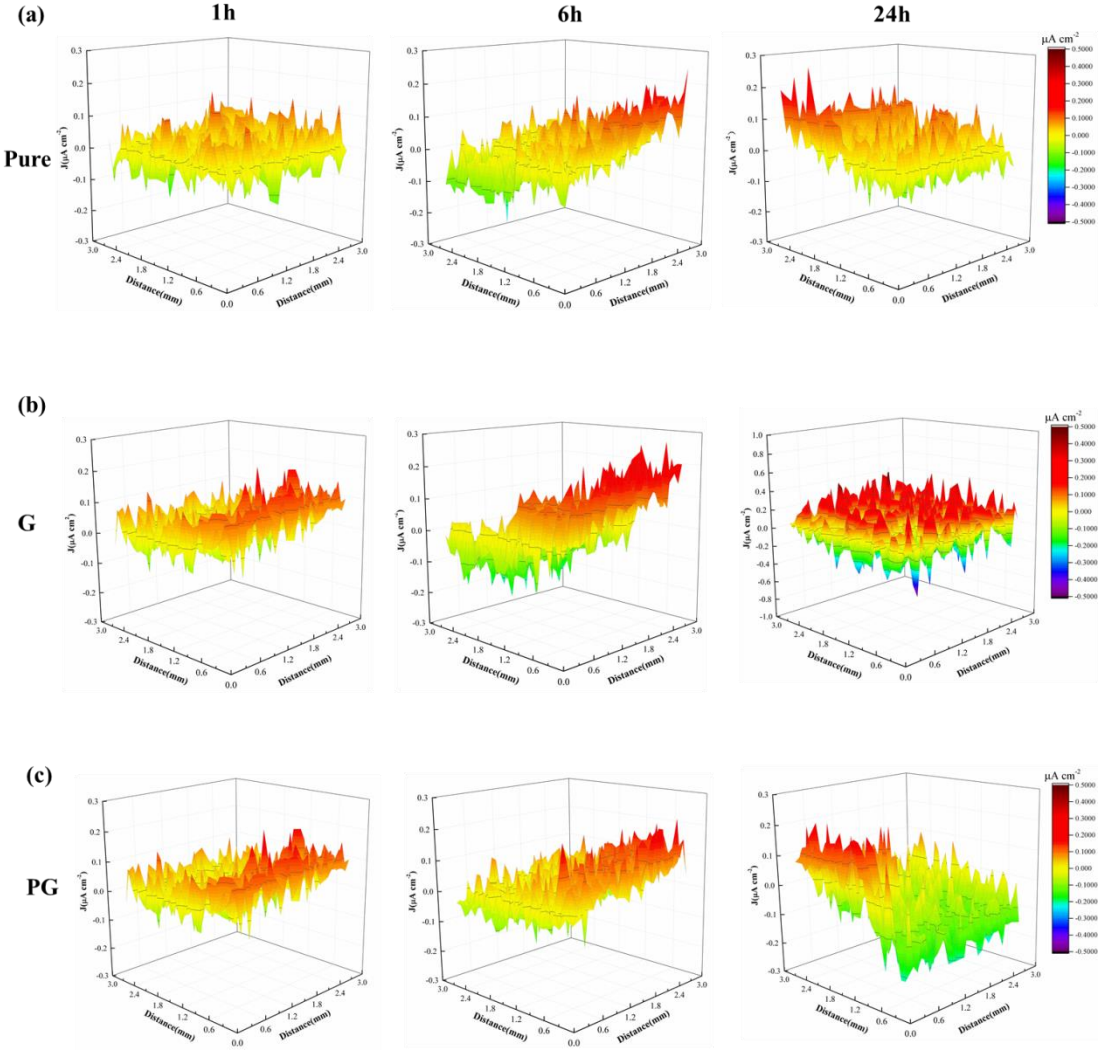

Figure 7. Current density distribution maps for coated steels immersed in 3.5 wt% NaCl solution for 1, 6 and 24 h: (a) pure , (b) G, and (c) PG

3.5 Salt spray test

In order to verify the corrosion resistance, the failure process of the composite coating was investigated by a salt spray test. The sample was exposed to a salt spray box of continuous spray (5 wt% NaCl solution) and maintained at a temperature of 35 ± 2 ˚C. It could be seen from Figure 8 that the surface corrosion deteriorated with the exposure time increased, and the surface of pure epoxy coating and G-coating layer were severely corroded, and the surface of PG-coating layer was not seriously corroded, indicating that PG-coating layer had excellent anticorrosive property [43].

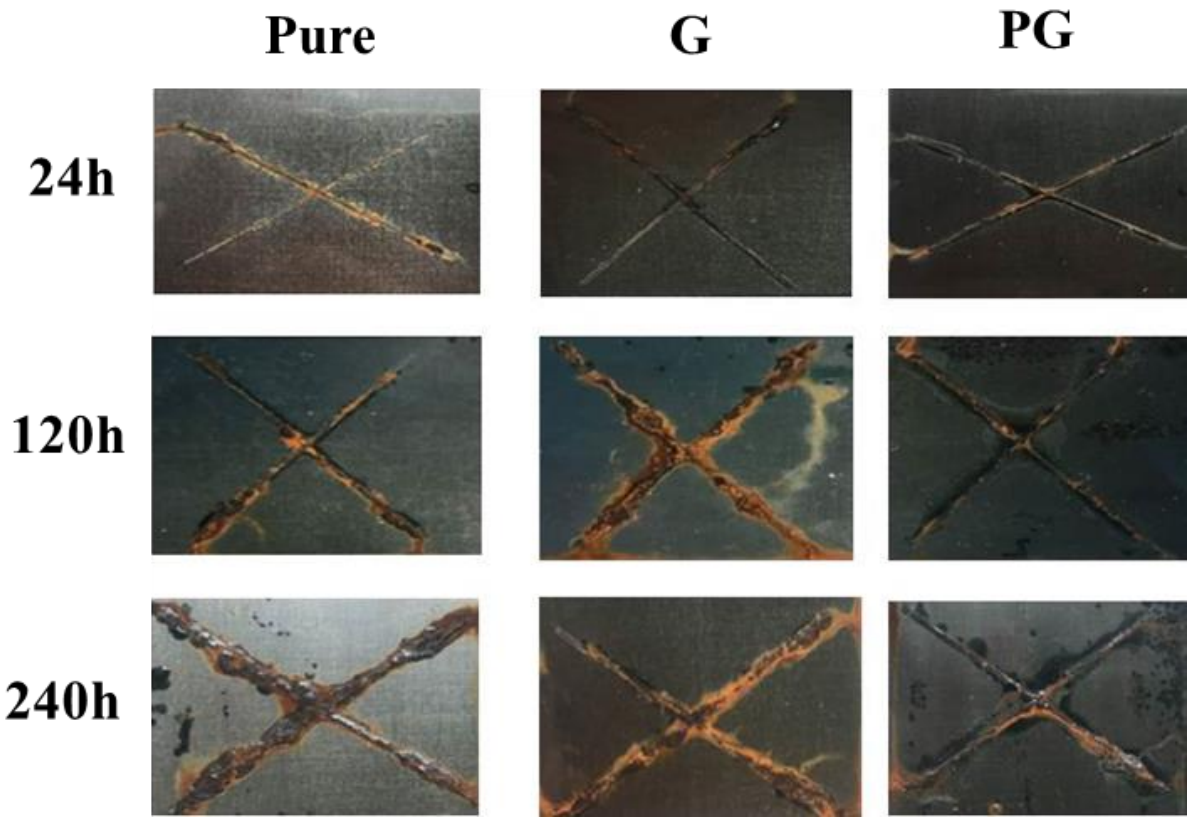

Figure 8. Optical photographs of pure-coating, G-coating and PG-coating after salt spray test.

3.6 Analysis of corrosion products

In Figure 9a, the corrosion products of the steel surface under the pure resin coating grew in the direction of pre-polishing, and the product was uneven and sparse; the corrosion product of the steel surface under the G-resin coating also grew in the direction of pre-polishing, but the products were denser than the former. The corrosion product under the PG-resin coating is entirely covered on the steel surface, and the dispersions were uniform and dense.

In Figure 9d, the corrosion products of pure epoxy resin consisted of α-Fe_2O_3 (227 cm^{-1}), γ-FeOOH (254 cm^{-1}), and α-FeOOH (397 cm^{-1}); the corrosion products of G-coatings were composed of γ-FeOOH (255 cm^{-1}), α-Fe_2O_3 (296 cm^{-1}), and α-FeOOH (398 cm^{-1}); the corrosion products of PG-coatings were all made up of Fe_3O_4 (667 cm^{-1}) [52-53].

The corrosion protection mechanism of the coating has been shown in Figure 10. On the basis of noncovalent interaction between PEDOT:PSS and graphene, agglomerated graphene is peeled off into 4-5 layers. The stripped graphene flakes has a good physical shielding effect, “labyrinth effect” increases the diffusion path of corrosive media; meanwhile PEDOT:PSS can accept electrons released by metal dissolution and reduce from oxidation state (doped form) to reduced state (dedoped form) [54], and the passivation layers of Fe_3O_4 are formed to protect the underlying metal from corrosion.

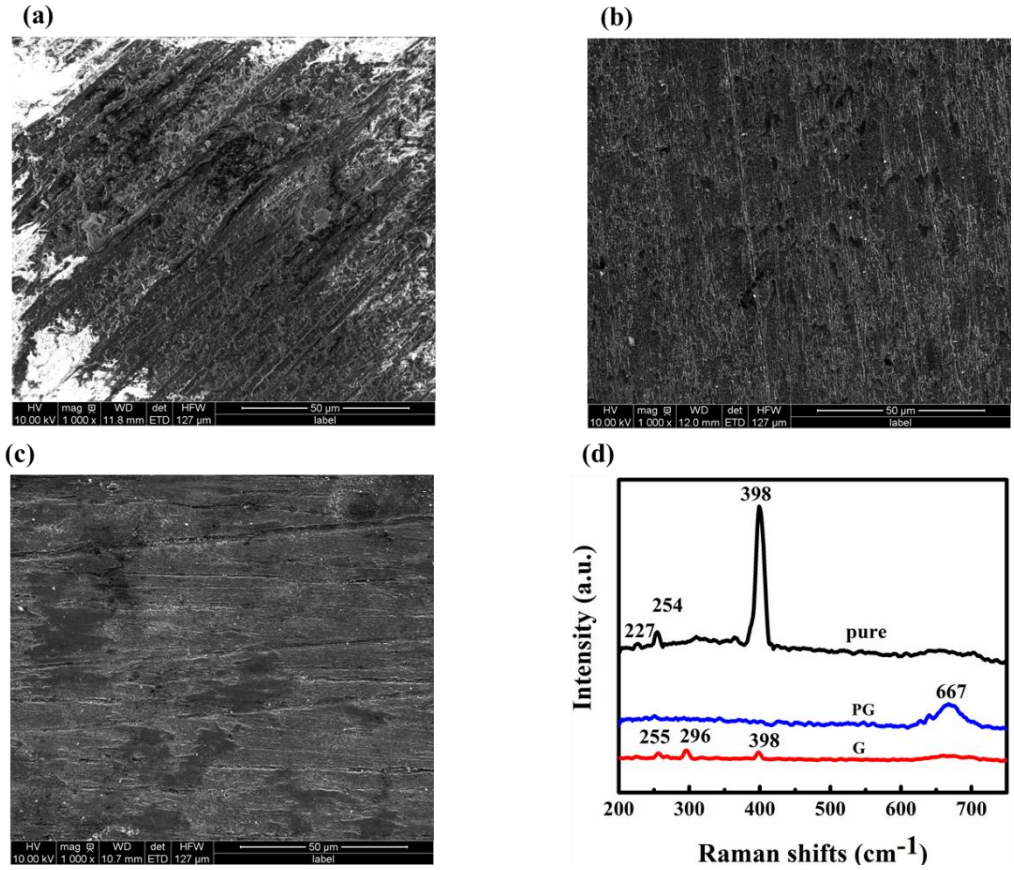

Figure 9. SEM images for rust regions on the steel substrate beneath (a) pure-coating, (b) G-coating and (c) PG-coating; (d) Raman spectra of the rust regions on the steel substrate beneath pure, G, and PG.

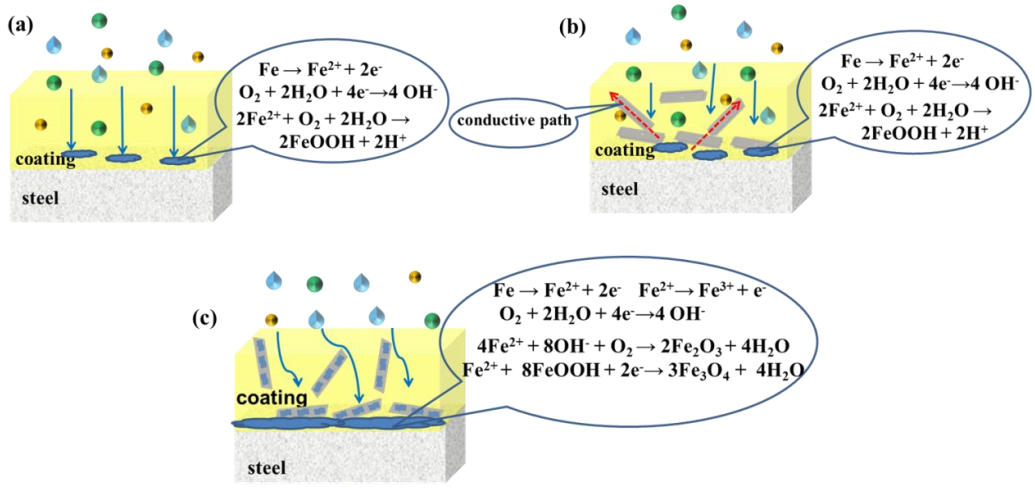

Figure 10. Corrosion protection mechanism for (a) pure-coating, (b) G-coating and (c) PG-coating.

4. CONCLUSION

In this paper, the PEDOT:PSS-G composites were prepared by a simple method. The PEDOT:PSS molecule is small in size and easy to insert into the graphene sheets. Graphene is stripped

into 4-5 layers of flakes by the π-π interaction between PEDOT:PSS and graphene.. Through XPS and Raman analysis, there is a π-π interaction between the two; XRD and TEM analysis found that the PEDOT:PSS molecule has been inserted into the graphene layer. Study on the electrochemical properties of the coating found that the agglomerated graphene had an accelerated corrosion phenomenon; while the exfoliated graphene acted as a labyrinth in the resin, which increased the diffusion path of the corrosive medium, furthermore PEDOT:PSS could be reduced from the doped state to the undoped state, and promoted the formation of the passivation layer of Fe_3O_4, so the progress of the corrosion reaction was suppressed. We hope that this highly efficient and excellent coating system can play a greater role in the field of corrosion protection.

ACKNOWLEDGMENTS
The authors gratefully thank the financial support provided by the National Science Fund for Distinguished Young Scholars of China (Grant No. 51825505); the "One Hundred Talented People" of the Chinese Academy of Sciences (No. Y60707WR04); Strategic Priority Research Program of the Chinese Academy of Sciences (XDA13040601); Natural Science Foundation of Zhejiang Province (No.Y16B040008).

References

1. S.Stankovich, D. A. Dikin, G. H. B.Dommett, K. M. Kohlhaas, E. J. Zimney, E. A. Stach, R. D. Piner, S. T. Nguyen, R. S. Ruoff, *Nature* ,442 (2006) 282.
2. J. C. Lei, Y. W. Hu, Z. S. Liu, G. J. Cheng, K. J. Zhao, *ACS Appl. Mater. Interfaces*, 9 (2017) 11902.
3. M. M. Zhu, Z. H. Du, Z. Y. Yin, W. W. Zhou, Z. D. Liu, S. H. Tsang, E. H. T. Teo, *ACS Appl. Mater. Interfaces*, 8 (2016) 502.
4. D. Prasai, J. C. Tuberquia, R. R. Harl, G. K. Jennings, K. I. Bolotin, *ACS Nano*, 6 (2012) 1102.
5. S. W. Zeng, K. V. Sreekanth, J. Z. Shang, T. Yu, C. K. Chen, F. Yin, D. Baillargeat, P. Coquet, H. P. Ho, A. V. Kabashin, K. T. Yong, *Adv. Mater*., 27 (2015) 6163
6. J. K. Wang, G. M. Xiong, M. M. Zhu, B.Ozyilmaz, A. H. C. Neto, N. S. Tan, C. Choong, *ACS Appl. Mater. Interfaces*, 7 (2015) 8275.
7. X. Z. Xu, D.Yi, Z. C. Wang, J. C. Yu, Z. H. Zhang, R. X. Qiao, Z. H. Sun, Z. H. Hu, P. Gao, H. L. Peng, Z. F. Liu, D. P. Yu, E. G. Wang, Y. Jiang, F. Ding, K. H. Liu, *Adv. Mater*., 30 (2018) 7.
8. S. Bohm, *Nat. Nanotechnol*., 9 (2014) 741.
9. S. S. Chen, L. Brown, M. Levendorf, W. W. Cai, S. Y. Ju, J. Edgeworth, X. S. Li, C. W. Magnuson, A. Velamakanni, R. D. Piner, J. Y. Kang, J. Park, R. S. Ruoff, *ACS Nano*, 5 (2011) 1321.
10. L. Nilsson, M. Andersen, R. Balog, E. Laegsgaard, P. Hofmann, F. Besenbacher, B. Hammer, I. Stensgaard, L. Hornekaer, *ACS Nano*, 6 (2012) 10258.
11. N. T. Kirkland, T. Schiller, N. Medhekar, N. Birbilis, *Corros. Sci*., 56 (2012) 1-4.
12. X. Li, W. Cai, J. An, S. Kim, J. Nah, D. Yang, R. Piner, A. Velamakanni, I. Jung, E. Tutuc, S. K. Banerjee, L. Colombo, R. S. Ruoff, *Science*, 324 (2009)1312.
13. M. Schriver, W. Regan, W. J. Gannett, A. M. Zaniewski, M. F. Crommie, A. Zettl, *ACS Nano*, 7 (2013) 5763.
14. F. Zhou, Z. T. Li, G. J. Shenoy, L. Li, H. T. Liu, *ACS Nano*, 7 (2013) 6939.
15. X. Luo, J. Zhong, Q. Zhou, S. Du, S. Yuan, Y. Liu, *ACS Appl. Mater. Interfaces*, 10 (2018) 18400.

16. X. Y. Li, P. Bandyopadhyay, T. Kshetri, N. H. Kim, J. H. Lee, *J. Mater. Chem.* A, 6 (2018) 21501.
17. B.Ramezanzadeh, G. Bahlakeh, M. Ramezanzadeh, *Corros. Sci*., 137 (2018) 111.
18. H. P. Zheng, M. Y. Guo, Y. W. Shao, Y. Q. Wang, B. Liu, G. Z. Meng, *Corros. Sci.* 139 (2018) 1.
19. C. Feng, L. J. Zhu, Y. Q. Cao, Y. Di, Z. X. Yu, G. H. Gao, *Int. J. Electrochem. Sci*., 13 (2018) 8827.
20. C. D. Yuan, M. Zhao, D. Sun, L. Yang, L. Zhang, R. W. Guo, F. L. Yao, Y. An, *J. Appl. Polym. Sci*., 135 (2018) 9.
21. T. Yang, Y. N. Cui, Z. S. Li, H. Zeng, S. Z. Luo, W. H. Li, *J. Hazard. Mater*., 357 (2018) 475-482.
22. C. Chen, S. H. Qiu, M. J.Cui, S. L. Qin, G. P. Yan, H. C. Zhao, L. P. Wang,; Q. J. Xue, *Carbon*, 114 (2017) 356.
23. S. H. Qiu, W. Li, W. R. Zheng, H. C. Zhao, L. P. Wang, *ACS Appl. Mater. Interfaces*, 9 (2017) 34294.
24. S. Timpanaro, M. Kemerink, F. J. Touwslager, M. M., De Kok, S. Schrader, *Chem. Phys. Lett*., 394 (2004) 339.
25. Y. Seekaew, S. Lokavee, D. Phokharatkul, A. Wisitsoraat, T. Kerdcharoen, C. Wongchoosuk, *Org. Electron*., 15 (2014) 2971.
26. G. Namkoong, E. M. Younes, T. M. Abdel-Fattah, E. M. El-Maghraby, A. H. Elsayed, A. H. A. Elazm, *Org. Electron*., 25 (2015) 237.
27. X. K. Wu, J. Liu, G. F. He, *Org. Electron*., 22 (2015) 160-165.
28. A. de Izarra, S. Park, J. Lee, Y. Lansac, Y. H. Jang, *J. Am. Chem. Soc*., 140 (2018) 5375.
29. J. Ouyang, Q. F. Xu, C. W. Chu, Y. Yang, G. Li, J. Shinar, *Polymer*, 45 (2004) 8443.
30. J. Y. Kim, J. H.Jung, D. E. Lee, J. Joo, *Synth. Met*., 126 (2002) 311.
31. M. H. Nazari, X. Shi, M. Hosseini, A. S. H. Makhlouf, Industrial Applications for Intelligent Polymers and Coatings, Springer, Cham (2016) Switzerland.
32. Y. W. Ye, D. W. Zhang, T. Liu, Z. Y. Liu, J. B. Pu, W. Liu, H. Zhao, X. Li, L. P. Wang, *Carbon*, 142 (2019) 164.
33. Y. W. Ye, D. W. Zhang, T. Liu, Z. Y. Liu, W. Liu, J. B. Pu, H. Chen, H. C. Zhao, X. G. Li, *J. Hazard. Mater.*, 364 (2019) 244.
34. W. Xing, Y. S. Chen, X. X. Wu, X. Z. Xu, P. Ye, T. Zhu, Q. Y. Guo, L. Q. Yang, W. W. Li, H.Huang, *Adv. Funct. Mater*., 27 (2017) 7.
35. K. N. Kudin, B. Ozbas, H. C. Schniepp, R. K. Prud'homme, I. A. Aksay, R. Car, *Nano Lett*., 8 (2008) 36.
36. D. Graf, F. Molitor, K. Ensslin, C. Stampfer, A. Jungen, C. Hierold, L. Wirtz, *Nano Lett.,* 7 (2007) 238.
37. Y. Y. Wang, Z. H. Ni, T. Yu, Z. X. Shen, H. M. Wang, Y. H.Wu, W. Chen, A. T. S. Wee, *J. Phys. Chem. C*, 112 (2008) 10637.
38. J. P. Thomas, L. Y. Zhao, D. McGillivray, K. T. Leung, *J. Mater. Chem*. A, 2 (2014) 2383.
39. D. Yoo, J. Kim, J. H. Kim, *Nano Res*., 7 (2014) 717.
40. G. H. Kim, D. H. Hwang, S. I. Woo, *Phys. Chem. Chem. Phys*., 14 (2012) 3530-3536.
41. P. B. Liu, Y. Huang, X. Sun, *ACS Appl. Mater. Interfaces*, 5 (2013) 12355.
42. S. Cho, M. Kim, J. Jang, *ACS Appl. Mater. Interfaces*, 7 (2015) 10213.
43. K. L. Xu, G. M. Chen, D. Qiu, *J. Mater. Chem*. A, 1 (2013) 12395.
44. Y. Li, H. Y. Chen, L. Y. Voo, J. Y. Ji, G. H. Zhang, G. L. Zhang, F. B. Zhang, X. B. Fan, *J. Mater. Chem.A*, 22 (2012) 15021.
45. C. H. L. Weijtens, V. van Elsbergen, M. M. de Kok, S. de Winter*, Org. Electron*. 6 (2005) 97.
46. J. W. Zhao, S. M. Xu, K. Tschulik, R. G. Compton, M.Wei, D. O'Hare, D. G. Evans, X. Duan, *Adv. Funct. Mater.* 25 (2015) 2745-2753.
47. C. B. Liu, H. C. Zhao, P. M. Hou, B. Qian, X. Wang, C. Y. Guo, L. P. Wang, *ACS Appl. Mater. Interfaces,* 10 (2018) 36229.
48. S. H. Qiu, C. Chen, W. R. Zheng, W. Li, H. C. Zhao, L. P. Wang, *Synth. Met*. 229 (2017) 39.
49. S. H. Qiu, C. Chen, M. J. Cui, W. Li, H. C. Zhao, L. P. Wang, *Appl. Surf. Sci*., 407 (2017) 213-222.

50. X. H. Luo, S. Yuan, X. Y. Pan, C. X. Zhang, S. Du, Y. L. Liu, *ACS Appl. Mater. Interfaces*, 9 (2017) 18263.
51. S. U. Ofoegbu, T. L. P. Galvao, J. R. B. Gomes, J. Tedim, H. I. S. Nogueira, M. G. S. Ferreira, M. L. Zheludkevich, *Phys. Chem. Chem. Phys*. 19 (2017) 6113.
52. X. H. Nie, X. G. Li, C. W. Du, Y. Z. Huang, H. Du, *J. Raman Spectrosc*. 40 (2009) 76.
53. X. Zhang, K. Xiao, C. F. Dong, J. S.Wu, X. G. Li, Y. Z. Huang, *Eng. Fail. Anal.* 18 (2011) 1981.
54. P. J. Kinlen, Y. Ding, D. C. Silverman, *Corrosion*, 58 (2002) 490.